Alloying with Sn Suppresses Sintering of Size-Selected Sub-Nano Pt Clusters on SiO_2 with and without Adsorbates

Borna Zandkarimi,[a,†] *Timothy J. Gorey,*[b,†] *Guangjing Li,*[b] *Julen Munarriz,*[a]

Scott L. Anderson,[b*] *Anastassia N. Alexandrova,*[a,c*]

[a]Department of Chemistry and Biochemistry, University of California, Los Angeles, 607 Charles E. Young Drive East, Los Angeles, CA 90095

[b]Department of Chemistry, University of Utah, 315 S. 1400 E., Salt Lake City, UT 84112

[c]California NanoSystems Institute, 570 Westwood Plaza, Los Angeles, CA 90095

[†]These authors contributed equally to this work.

[*]Senior Authors

Corresponding Authors: Scott Anderson, (801) 585-7289, anderson@utah.edu, Anastassia Alexandrova, (310) 825-3769, ana@chem.ucla.edu

ABSTRACT

Using Pt in the form of sub-nanometer dispersed clusters is a way to save precious metal in catalysis, but making such clusters stable against sintering is an uphill battle. Sn is a known agent used to increase the selectivity of dehydrogenation of alkanes on Pt. Through a joint experimental and theoretical approach, we show that adding Sn to the size-selected Pt clusters deposited on amorphous SiO_2 also dramatically enhances the thermal stability of the clusters against sintering. CO temperature programmed desorption (TPD) and He^+ ion scattering indicate that no Pt sites are lost, and XPS shows no change in the electronic structure of Pt, upon repeated system heating and cooling. DFT results indicate that the binding energy of Pt clusters to the support increases by >1 eV upon adding Sn, and Sn forms strong polar covalent bonds with Pt within the clusters and quenches all the unpaired spins. As a result, the energy needed to remove a Pt atom from Pt_4Sn_3/SiO_2 and put it on the support is 0.15 eV larger than that from Pt_4/SiO_2, and in fact it is significantly easier to dissociate a Sn atom. Both factors would tend to stabilize the Pt core of the clusters against sintering, as is observed experimentally. CO adsorbates further facilitate Ostwald ripening of the pure Pt clusters, and even in that case nano-alloying with Sn suppresses sintering.

INTRODUCTION

Catalysis at the interface has increasingly been used in many fields, ranging from chemical industry and manufacturing to the rapidly growing areas of energy generation and storage.[1,2] An important approach to improving the activity per mass of precious metal is decreasing the metal particle size to the sub-nanometer range, such that most, if not all, of the precious metal atoms are available in the surface layer. However, sub-nano catalysts tend to sinter more rapidly than catalysts with larger particles, because the small clusters are thermodynamically less stable, and have fewer metal-metal and metal-substrate bonds stabilizing them.[3–5] For instance, it has been shown that isolated adatoms of Ag, Cu, and Pd on oxide supports such as MgO(100) are extremely mobile at ambient temperature, and diffuse swiftly across the support until they join a growing metal cluster.[6] Sub-nano catalysts may also poison more rapidly due to the low coordination of the cluster atoms. There are many ways that have been considered for sintering prevention.[3,7–10] One way is by doping or co-alloying of precious metals with other elements to favorably modify its electronic structure. It has been suggested that, when used at a proper ratio, Pd can be used as a dopant in order to decrease Pt clusters sintering on TiO_2(110).[11,12] For PtPd, the effect was attributed to electronic and also entropic effects of mixing.[11] Boron can also be used to increase the stability of Pt clusters on MgO as predicted by theory,[13] and on α-Al_2O_3(0001) as shown by both theory and experiment.[14] Borating small Pt clusters on alumina supports leads to significantly suppressed ethylene dehydrogenation, and therefore also

reduced the tendency of the clusters to become poisoned by carbon deposition. In addition, Si and Ge were proposed to be promising dopants for the same purpose, but so far only from theory.[15,16]

Undoubtedly, Sn is one of the most well-known dopants for Pt that reduces sintering in larger nanoparticles deposited on different surfaces, including γ-Al_2O_3 and SiO_2.[17–22] For example, using XPS and EXAFS, Siri et al. showed that bimetallic PtSn/γ-Al_2O_3 catalysts after several sequential reaction–regeneration cycles have the same level of initial activity each time, demonstrating that the nature of the catalytic surface remains practically unmodified.[23] This is despite the fact that Sn has low melting and boiling points (mp (Sn) = 505.08 K, bp (Sn) = 2875 K), thus one might expect that Sn alloying might reduce the thermal stability of refractory precious metals such as Pt (mp(Pt) = 2041.4 K, bp(Pt) = 4098 K). In fact, a strong Pt-Sn interaction will improve the stability of the catalysts operating at harsher conditions, as was shown by Pastor-Pérez et al.[24] We recently presented a method of preparation of model catalysts with size-selected Pt clusters decorated by controlled coverage of Sn atoms, which are shown to alloy upon heating.[25]

The effects of Sn on catalytic activity and stability of sub-nano Pt clusters has been less studied. Smaller clusters are most prone to sintering, and that often precludes their use in practical catalysis, with the rate of sintering depending on particle size and support material.[26] We previously showed that Sn-alloying reduced the coking tendency of sub-nano Pt clusters

on SiO_2,[27] and alumina,[28] although for alumina Sn was deposited non-selectively on both the support and clusters. In those studies, the ethylene TPD behavior was found to be more stable from run to run than that for analogous pure Pt clusters, suggesting that the cluster had enhanced stability relative to both coking and sintering. Here, we directly probe the stability of PtSn clusters on SiO_2, and show that, indeed, they do have enhanced stability with respect to sintering. Sintering is largely suppressed for the smallest cluster sizes considered, and abated for larger clusters, as probed by a combination of carbon monoxide temperature-programmed desorption (CO-TPD), X-ray photoelectron spectroscopy (XPS), ion scattering spectroscopy (ISS), temperature-dependent XPS, (TD-XPS), temperature-dependent ISS (TD-ISS), as well as theoretical calculations. The theory must address these systems as statistical ensembles of many thermally-accessible states at experimental temperatures, rather than just the global minimum.[29,30] Indeed, in recent studies, we showed that this approach is essential to describe properties of cluster catalysts, including sintering propensity.[13,31] Details of the experimental and theoretical protocols are given in the SI.

METHODS

Experimental. Details can be found in the SI. In brief, experiments were done using an instrument described previously,[32,33] that includes a cluster source that allows deposition of atomically size-selected metal

clusters onto planar supports in ultrahigh vacuum (UHV, base pressure = 1.0 x 10^{-10} Torr). The instrument is equipped for *in situ* X-ray and UV photoelectron spectroscopy (XPS/UPS), low-energy He^+ scattering spectroscopy (ISS), temperature-programmed desorption (TPD), and has an antechamber used for sample exchange and dosing of gasses for Sn deposition. Model catalysts were prepared on 10 mm × 14 mm pieces of oxidized Si(100), which we will simply refer to as "SiO_2 substrates". For each experiment, a fresh SiO_2 substrate was inserted into the antechamber was evacuated overnight, then cleaned by annealing at 700 K under 5.0 x 10^{-6} Torr oxygen, followed by 2 minutes of 700 K annealing in UHV, resulting in a surface oxide layer measured to be ~1.1 nm thick. Pt_n/SiO_2 samples were prepared by depositing Pt_n^+ clusters onto clean SiO_2 substrates, with coverage set to 1.5 x 10^{14} Pt atoms/cm^2 for all samples, equivalent to ~10% of a close-packed Pt monolayer. For this study, we examined Pt_4, Pt_7, Pt_{12}, and Pt_{24} clusters. Pt_4 was chosen for theoretical tractability and as a representative small cluster. Pt_7 was chosen because it represents a transition to 3D multilayer structure,[25,32,34] and Pt_{12} and Pt_{24} were chosen to examine changes for intermediate and larger cluster sizes.

Preparation of Pt_nSn_x/SiO_2 alloy clusters is described in the SI, and characterization is given elsewere.[25] In essence, size-selected Pt_n deposited on SiO_2 are used to seed selective addition of Sn, by exposing the samples to H_2, then $SnCl_4$, which binds preferentially to the hydrogenated Pt sites, then again to H_2 to remove Cl as HCl. Sn deposition is selective and self-limiting,

i.e., Sn deposits on hydrogenated Pt sites hundreds of times more efficiently than on the SiO_2 substrate, and increasing the $SnCl_4$ exposure results in no increase in the Sn:Pt ratio, which is found to be just over 1:1 for smaller clusters ($Pt_4Sn_{3.3}$, $Pt_7Sn_{6.3}$) becoming more Pt-rich for the larger clusters ($Pt_{12}Sn_8$, $Pt_{24}Sn_{7.5}$). The change in stoichiometry is attributed to a size-dependent change in Pt_n structure from single layer to multilayer, thus exposing fewer Pt sites.

CO binds strongly to Pt clusters,[10,34] thus CO TPD is a useful probe of the number and energetics of reactant-accessible Pt binding sites, and their evolution in multiple TPD runs. For each TPD run, the sample was cooled to 180 K, exposed to 10 L of ^{13}CO, then the temperature was ramped at 3 K/s to 700 K, while monitoring signals of interest ($^{13}CO^+$, D_2^+, H_2O^+, $^{12}CO^+$, $H^{35}Cl^+$, $^{12}CO_2^+$, $^{13}CO_2^+$, and Cl_2^+) using a differentially pumped mass spectrometer. The 180 K CO dose temperature was chosen as being low enough to populate Pt sites while minimizing adsorption on SiO_2 and Sn sites. Measured $^{13}CO^+$ intensity vs. temperature was converted to absolute numbers of desorbing molecules by calibrating the detection efficiency using known fluxes of CO into the mass spectrometer. For calibration of HCl detection efficiency, Ar, which has similar mass and ionization efficiency, was used. We conservatively estimate the *absolute* uncertainty in TPD calibration to be ±50 %, with relative uncertainty for comparing different experiments of ~±15%. The CO TPD data were fit to extract desorption energies as described in the SI.

A temperature-dependent ISS (TD-ISS) method was used to probe adsorbate binding sites and thermally induced changes to cluster morphology. For TD-ISS, freshly prepared samples were moved to the ISS position, set to 180 K, and then dosed with CO. ISS spectra were then taken at a series of increasing temperatures to observe changes in the Pt ISS intensity due to CO desorption and morphology changes to the Pt. Some experiments were done on samples that were first subjected to a normal CO TPD run, and control experiments were done without CO dosing and without heating to estimate Pt and CO sputtering effects. To minimize sputter damage by He^+, low currents (0.3 μA) were used. A similar process was used for TD-XPS experiments, recording Pt 4f and Sn 3d signals as a function of temperature to observe changes in binding energies and intensities.

Computational. The structures of the Pt_4, Pt_4Sn_3, Pt_4/SiO_2, Pt_3/SiO_2, Pt_4Sn_3/SiO_2, and Pt_4Sn_2/SiO_2 clusters, with and without adsorbed CO, were obtained through global optimization, done at the plane wave DFT (PW-DFT) level, using projector augmented wave (PAW) potentials[35] and the PBE[36] functional, as implemented in Vienna Ab initio Simulation Package (VASP).[37-40] The cut-off energy for plane waves used in this study was 400.0 eV and the convergence criteria for electronic relaxations was 10^{-6} eV. Geometric relaxation was performed until forces on atoms were smaller than 0.01 eV/Å. Gaussian smearing with a sigma value of 0.1 eV was used for all calculations. For Pt_4 and Pt_4Sn_3 clusters in gas phase, a unit cell of 20 Å × 20 Å × 20 Å was used to perform PW-DFT. For the surface-supported calculations the bottom

half of the slab was kept fixed. The SiO_2 slab structure was taken from that of bulk amorphized cristobalite and was previously optimized[41] at the B3LYP/ 6-31G(d,p)[42–45] level of theory. The cell parameters used in this study are a = 12.4 Å, b = 13.1 Å, c = 32.0 Å, α = 90°, β = 90°, and γ = 88°, and slabs were separated by a 14 Å vacuum gap. Due to the large supercell used in this study, only the Γ-point sampling was used to obtain the energy. A cut-off energy of 0.4 eV and Boltzmann statistics were used to identify the thermally-accessible isomers at relevant temperatures, as we showed (through great computational expense) that most of the thermodynamically accessible isomers of Pt cluster on oxides should also be kinetically accessible on the time-scales relevant to catalysis.[46] In order to produce initial geometries for clusters on the SiO_2 surface at the initiation of sampling, we use our in-house parallel global optimization and pathway toolkit (PGOPT),[47] which automatically generates these structures based on the bond length distribution algorithm (BLDA). Each structure was optimized with DFT and duplicates were recognized and removed. Partial charges on each atom in the cluster were obtained using the Bader charge scheme.[48–51] The global minima were additionally confirmed by basin hopping global optimization separately.[52] More detailed discussion of methods can be found in the SI.

RESULTS AND DISCUSSIONS

I. DFT Analysis of PtSn Clusters

DFT global optimization of gas-phase Pt_4 and Pt_4Sn_3 reveals that alloying with Sn is likely to strongly stabilize Pt clusters due to a specific electronic effect (**Fig. S1**). All but one Pt_4 isomers thermally-accessible at 700 K (according to Boltzmann statistics; 0.4 eV energy cutoff), including the global minimum, are open-shell system, triplets and quintets. In contrast, 10 out of the 13 thermally-accessible isomers of Pt_4Sn_3 are closed-shell, and have the Pt and Sn atoms interspersed rather than phase separated. This implies that the valence orbitals of Sn and Pt match well in energy and spatial extent, allowing them to pair and form strong Pt-Sn bonds.

The low energy isomers found for Pt_4/SiO_2 and Pt_4Sn_3/SiO_2 are shown in **Fig. 1a,b**. For Pt_4/SiO_2, the four lowest energy isomers are shown, however, note that only structures I and II are below the 0.4 eV energy cut-off used for the gas-phase clusters, and these are just triplet and singlet versions of the same cluster geometry. The singlet state II is actually open-shell di-radical, and results in I upon flipping the spin, with essentially no effect on the bonding or electron density distribution (see **Fig. S2**). Isomers I and II are only 0.039 eV apart, and so the population of II becomes significant at temperatures relevant to the experiments. Hence, the average spin state of this system is predicted to be temperature dependent. The optimized structures are bound to the surface with both Pt-Si and Pt-O bonds, and all are approximately planar, with the cluster plane oriented roughly perpendicular to the SiO_2 surface plane for the three lowest energy

structures, and roughly parallel for isomer IV. The structures all have one Pt atom with a significant negative Bader charge (up to -0.64e), one or two atoms with the charges near zero, and one or two with significantly positive charges (up to +0.47e). The net charge on the cluster is -0.1e for the two structures with significant thermal populations (**Table 1**), and the net charges for the two higher energy isomers are -0.1e and -0.06e.

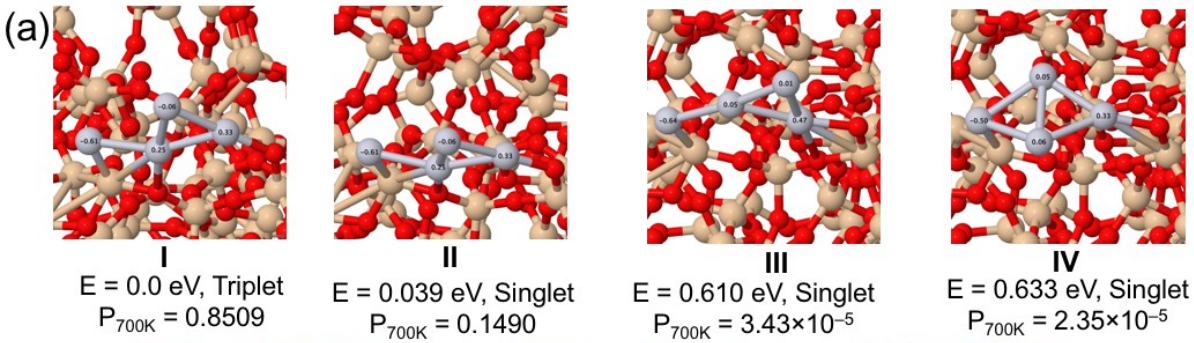

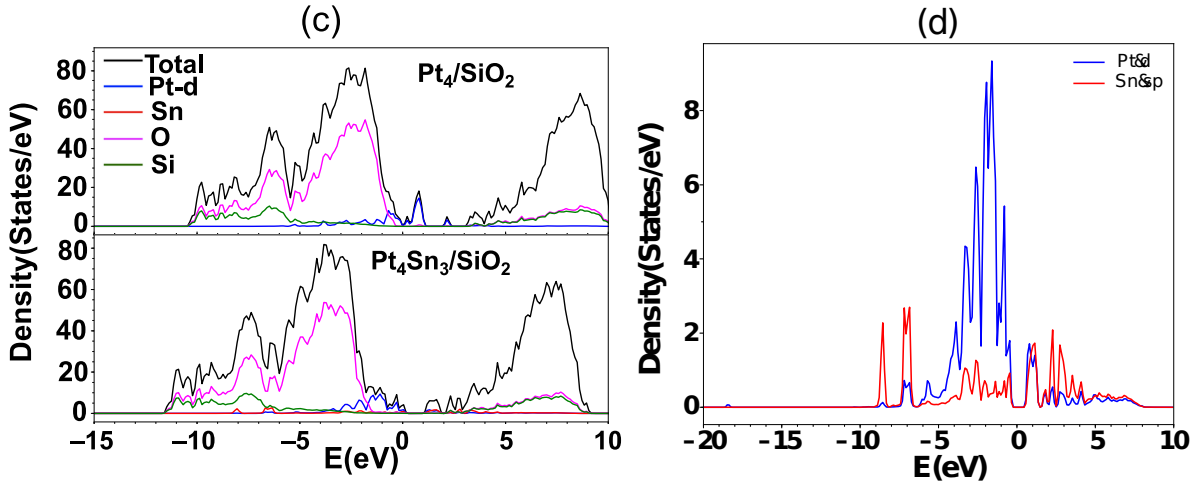

Figure 1. The geometry and spin state of local minima structures of (a) Pt_4 and (b) Pt_4Sn_3 clusters deposited on SiO_2 along with their corresponding Boltzmann population at 700 K obtained from DFT calculations. Results shown in (b) are adopted from Ref. [25]. Charge on each atom is calculated using Bader charge scheme. Note that the singlet Pt_4 structure is 4° more away from the vertical line (tilted forward) than the global minimum structure. (c) Total and site-projected spin-up density of states of Pt_4Sn_3/SiO_2 and Pt_4/SiO_2, shown in black (total), blue (Pt), red (Sn), green (Si), and magenta (O). (d) Zoom at the Pt- and Sn-projected spin-up density of states of Pt_4Sn_3/SiO_2 shows the interaction between Pt d orbitals and Sn valence orbitals resulting in quenching the unpaired electrons on Pt_4.

For Pt_4Sn_3/SiO_2 (**Fig. 1b**),[25] only three thermally-accessible structures were found, compared to 13 for gas-phase Pt_4Sn_3. It appears that binding to SiO_2 substantially suppresses the number and diversity, i.e. fluxionality of these clusters compared to the gas phase, as might be expected. Furthermore, the global minimum of Pt_4Sn_3/SiO_2 strongly dominates the population at all temperatures because it is significantly more stable than the other isomers. The two lowest energy isomers both bind to the surface via Pt atoms, and for all three isomers there are at least three Pt atoms with substantially negative charges (up to -0.85e). The global minimum isomer and isomer III have no positively charged Pt atoms. Isomer II has one that is just above zero (0.07e). The charges for all Sn atoms in all isomers are substantially positive (up to 0.93e), i.e., there is significant Sn-to-Pt electron transfer, reflecting the greater electronegativity of Pt. The net charge on the Pt_4Sn_3 cluster (**Table 1**) is positive (+0.29 to +0.42e), i.e., the presence of Sn reverses the direction of cluster-substrate electron transfer.

Table 1. Energy, Bader charge, spin multiplicity, and Boltzmann populations at 450 K and 700 K of thermally-accessible isomers of Pt_4/SiO_2 and Pt_4Sn_3/SiO_2 obtained from DFT calculations.

Isomer	E(eV)	ΔQ(e)	2S+1	P(450 K)	P(700 K)
Pt_4-I	0	–0.10	3.0	0.89	0.85
Pt_4-II	0.039	–0.10	1.0	0.11	0.15
Pt_4Sn_3-I	0	0.42	1.0	0.97	0.91
Pt_4Sn_3-II	0.135	0.29	1.0	0.026	0.089
Pt_4Sn_3-III	0.356	0.31	1.0	9.1×10^{-5}	0.0023

As with the gas phase clusters, addition of Sn to the SiO_2-supported Pt clusters tends to quench the spin, such that all thermally accessible structures are singlets. This effect on the spin was also found for Si and Ge as co-alloying elements for Pt clusters, predicted to discourage dehydrogenation of hydrocarbons beyond olefins.[15,16] The total and site-projected density of states (DOS and PDOS) of Pt_4/SiO_2 and Pt_4Sn_3/SiO_2 were calculated to further illustrate this (**Fig. 1c**). By comparing the spin-up DOS and PDOS of Pt_4Sn_3/SiO_2 and Pt_4/SiO_2 near the Fermi level (E_F), one can easily see the decrease in the intensity of the near-E_F Pt PDOS when Sn is added to the cluster. This attenuation reveals the Pt-Sn bonding and the drop of these bonding states to lower energies. At the same time, the spins on Pt are quenched, as is demonstrated by the symmetrizing of the α and β PDOS on Pt upon Sn addition (see **Fig. S3** and **S4**). Again, the spin quenching is suggestive of strong intra-cluster bonding (one indication of likely sintering suppression).

To evaluate the propensity of clusters to Ostwald ripening, we computed the ensemble-average intra-cluster binding energies - the energies required to dissociate one atom (Pt or Sn) from the cluster and put it on the most favorable site on the surface ($E_{clust,bind}$, **Table 2**). To do this, we also performed global optimizations of the product states, Pt_3/SiO_2, Pt/SiO_2, Pt_4Sn_2/SiO_2, Pt_3Sn_3/SiO_2, and Sn/SiO_2, sampling both the cluster geometries and the binding sites on the support (see **Figs. S5-S7**). Moving a Pt atom from Pt_4/SiO_2 to the support costs only ~0.32 eV, whereas for Pt_4Sn_3/SiO_2 the energy cost is calculated to be ~50% higher. On the other hand, removing Sn from Pt_4Sn_3/SiO_2 to the support costs only ~0.3 eV, i.e., roughly the same energy as that needed to remove Pt from Pt_4/SiO_2. Hence, the calculations suggest that Sn atoms might dissociate from the Pt_nSn_m clusters at high temperatures and migrate to other clusters, but the Pt core of the clusters is likely to remain intact as long as the cluster contains some Sn. This suggests that Pt should be sintering resistant in the presence of Sn, even though Sn itself might be mobile.

Table 2. Ensemble-averaged intra-cluster binding energy ($E_{clust,bind}$) and binding energies to SiO_2 ($E_{surf,bind}$) of Pt_4 and Pt_4Sn_3 calculated at relevant temperatures (see computational methods for formulas). For Pt_4Sn_3 the values in parenthesis correspond to the energy required to remove one Sn atom from the cluster.

Cluster	$E_{clust,bind}$(eV)		$E_{surf,bind}$(eV)	
	450 K	700 K	450 K	700 K
Pt_4/SiO_2	0.32	0.31	–6.14	–6.17
Pt_4Sn_3/SiO_2	0.47(0.31)	0.46(0.29)	–7.25	–7.26

DFT also finds that Sn significantly strengthens the binding of the Pt clusters to the surface ($E_{surf,bind}$(eV), **Table 2**), although even the pure Pt_4 clusters are quite strongly bound. There is a ~1.1 eV ensemble-average increase in the binding energy of the cluster to the surface upon addition of Sn. There is no particularly enhanced covalent overlap between the states of the support and the states on Pt or Sn. Thus, we attribute the strengthening of the PtSn-SiO_2 bonding to the increase in the absolute charge transfer between the cluster and support, which increases binding by the Columbic attraction. In addition to thermodynamic stabilization, the effect would also tend to increase the barriers to diffusion across the ionic SiO_2 surface, because the system would have to pass through regions of repulsive ionic interactions and/or reorganize electronically and geometrically. Thus, the theoretical findings indicate that Sn alloying should tend to stabilize sub-nano Pt clusters against sintering by several mechanisms.

II. Surface Analysis using ISS and XPS

To experimentally assess the stability of the clusters with respect to thermal sintering, we carried out temperature-dependent ISS (TD-ISS) and XPS (TD-XPS) experiments on as-deposited, adsorbate-free Pt_4/SiO_2 and Pt_{12}/SiO_2 samples (**Fig. 2**). In each experiment, the sample was cooled to

180 K, then heated in 50 K steps, taking ISS, or XPS scans over the Pt 4f, Si 2p, and O 1s regions, at each temperature. **Fig. 2a** plots the temperature dependence of the Pt 4f binding energy (BE), the Pt 4f : Si 2p XPS intensity ratio, and the Pt ISS intensity, normalized to total scattered intensity, which is dominated by Si and O. The horizontal dashed lines show the Pt 4f BEs for as-deposited Pt_4/SiO_2, Pt_7/SiO_2, Pt_{12}/SiO_2, and Pt_{24}/SiO_2, which grow by ~1 eV as cluster size decreases, due to the size-dependent stabilization of the photoemission final state.[53,54] For reference, the Pt 4f BE for bulk Pt is generally reported to be ~71 eV.[55]

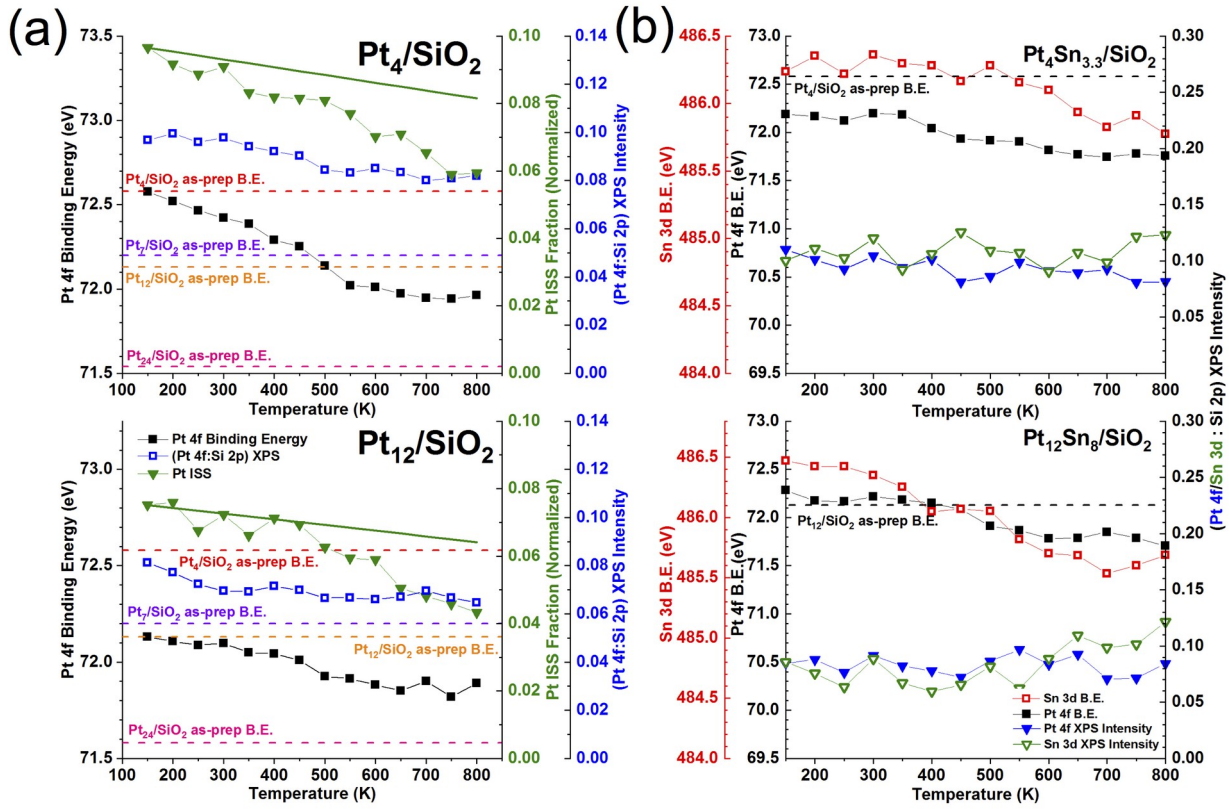

Figure 2. (a) TD-XPS of the Pt 4f binding energy (solid black squares), the normalized Pt XPS intensity ratio (hollow blue squares), and temperature-dependent Pt ISS (TD-ISS) of bare, as-deposited clusters (solid green triangles), for Pt_4/SiO_2 (top) and Pt_{12}/SiO_2 (bottom). Solid green lines are

overlaid showing the expected loss in Pt ISS due to sputtering. (b) TD-XPS of the Pt 4f binding energy (solid black squares), Sn 3d (red hollow squares), TD changes in the Pt 4f:Si 2p (blue triangle) and Sn 3d (green hollow triangle) XPS intensity ratios, for $Pt_4Sn_{3.3}/SiO_2$ (top) and $Pt_{12}Sn_8/SiO_2$ (bottom). For reference, as-deposited Pt_n/SiO_2 4f binding energies are plotted as dashed lines.

For Pt_4/SiO_2, the Pt 4f BE decreased by ~0.6 eV as the sample was heated to 550 K, then decreased more slowly between 550 K and 800 K. The BE dropped below those measured for as-deposited Pt_7 and Pt_{12} at ~450 K, but remained well above the BE for as-deposited Pt_{24}/SiO_2. The decrease in Pt 4f BE is consistent with Pt_4 sintering into larger clusters, and the fact that the final BE is between those for as-deposited Pt_{12} and Pt_{24} suggests that the final average size was between 12 and 24 atoms. The Pt 4f : Si 2p intensity ratio was roughly stable up to ~300 K, then declined monotonically at higher temperatures, consistent with previous studies of Pt_n/SiO_2.[54] An overall ~20% loss was observed. Some decrease in the Pt:Si XPS intensity ratio is expected from sintering into multilayer clusters, both because Pt would cover less of the SiO_2 surface, increasing the Si intensity, and because Pt XPS from atoms sub-surface layers would be attenuated.

The normalized Pt ISS intensity dropped by ~39% as the sample was heated, and the decrease rate was approximately constant. This is a measure of the number of exposed Pt atoms, and we previously reported[25] that the Pt ISS signal decreased substantially with increasing cluster size, in the ratio 1.0 : 0.50 : 0.37 for Pt_4 : Pt_7 : Pt_{24} (Pt_{12} was not included in this study). ISS peak intensities primarily reflect He^+ scattering from individual Pt

atoms in the surface layer of the clusters.[56–59] Therefore, the decreasing Pt ISS intensities suggest that, as cluster size increases, the cluster structures become increasingly multilayer, such that smaller fractions of the Pt atoms are in the top layer. Note that some loss of ISS intensity is expected due to sputtering of Pt from the surface by the 1 keV He^+ beam used for ISS. The average sputter loss rate (green line, **Fig. 2a**) was measured by exposing a fresh Pt_4/SiO_2 sample to the ISS beam at constant temperature, and taking the beam exposures into account. The TD-ISS intensity decreases more rapidly than the loss from spattering, and for Pt_4 it occurs over the entire temperature range, while for Pt_{12} it starts after ~450K. Hence, both clusters exhibit significant thermal changes that reduce the fraction of Pt atoms in the top layer. Note that, in another study, sintering upon annealing of Pt_2, Pt_{13}, and Pt_{24} on SiO_2 was detected by XPS, grazing-incidence X-ray absorption near-edge spectroscopy (XANES) and grazing-incidence small angle X-ray scattering (GISAXS).[54] This work showed that small Pt_n/SiO_2 are stable at room temperature, and increase in apparent size starting at 423 K, consistent with our observations.

TD-XPS and TD-ISS experiments were also performed on $Pt_4Sn_{3.3}/SiO_2$, and $Pt_{12}Sn_8/SiO_2$ under conditions identical to those used for the experiments on Pt_4/SiO_2 (**Fig. 2b**). These experiments were done for as-prepared $Pt_4Sn_{3.3}/SiO_2$ and $Pt_{12}Sn_8/SiO_2$ prior to the final heating step used to desorb residual Cl and H,[25] therefore the TD-ISS signals for Cl and H were also monitored. TD-XPS upon the first heating was also affected by Cl and H. For both cluster

sizes, the Pt 4f BE is roughly constant up to 350 K, then decreases significantly at 400 K becoming constant again above ~650 K. The range where the BE drops most rapidly is where HCl desorption and loss of Cl ISS signal is observed,[25] and thus the drop in Pt BE is attributed primarily to desorption of Cl – an electron-withdrawing adsorbate. For $Pt_4Sn_{3.3}$, the Pt 4f:Si 2p intensity ratio drops slowly over the entire temperature range, but only by ~3%, compared to the ~15% drop observed for Pt_4/SiO_2 (**Fig. 2a**). For $Pt_{12}Sn_8$, there was no significant change in the intensity ratio over the full temperature range, in contrast to the bare Pt_{12}/SiO_2, which showed a ~20 % drop. The Sn BE drops slowly up to 500 K, but then drops more rapidly between 500 and ~700 K. This drop in BE appears to be correlated with an increase in Sn 3d ISS intensity for both sizes. Most desorption is complete by ~600 K, and the Sn ISS intensity, which also increases between 500 and 600 K, drops at higher temperatures. It is not clear what changes occur in the >600 K range, but most likely they involve changes in the morphology of the clusters, Sn migration between the clusters (predicted by theory, **Table 2**), and possibly some sintering. Overall, experiment and theory agree that the adsorbate-free Pt clusters are significantly less susceptible to thermal sintering when alloyed with Sn.

III. CO TPD

It is arguably more important that cluster withstand sintering when they are covered with adsorbates in reaction conditions. To probe this, we

performed a series of ^{13}CO TPD experiments. CO is not just a relevant carbonaceous adsorbate, but also is a useful TPD probe that binds strongly to Pt clusters,[10,34] and reports on the number and energetics of reactant-accessible Pt binding sites. CO TPD after 180 K CO exposure was performed for a Pt-free SiO_2 substrate, and for Pt_4/SiO_2, Pt_7/SiO_2. Pt_{12}/SiO_2, and Pt_{24}/SiO_2. Multiple TPD runs, each with 180 K CO exposure, were run to assess changes in the CO binding site distribution driven by the TPD process (**Fig. 3a**). CO^+ counts/second have been converted to molecules desorbing *per* degree (the intensity scale be divided by the 3K/second heating rate), and molecules desorbing *per* second using the calibration process described above.

CO desorption from SiO_2 occurred exclusively at low temperatures, beginning at the onset of the heat ramp (180 K), peaking near 250 K, and going to completion by ~350 K. Upon extending the heating to 1000 K, no additional CO desorption was observed and no run-to-run changes were observed. The integrated amount of CO desorbing was found to be ~1.0 x 10^{13} molecules/cm^2, i.e. roughly a percent of a close-packed monolayer, suggesting that desorption from SiO_2 in this temperature range is confined to a few high-affinity sites on the amorphous SiO_2 surface. When CO dosing was done at 150 K, a much larger number of CO molecules desorbed from SiO_2. More detailed discussion of the TPD spectra and the nature of the peaks can be found in Note S5

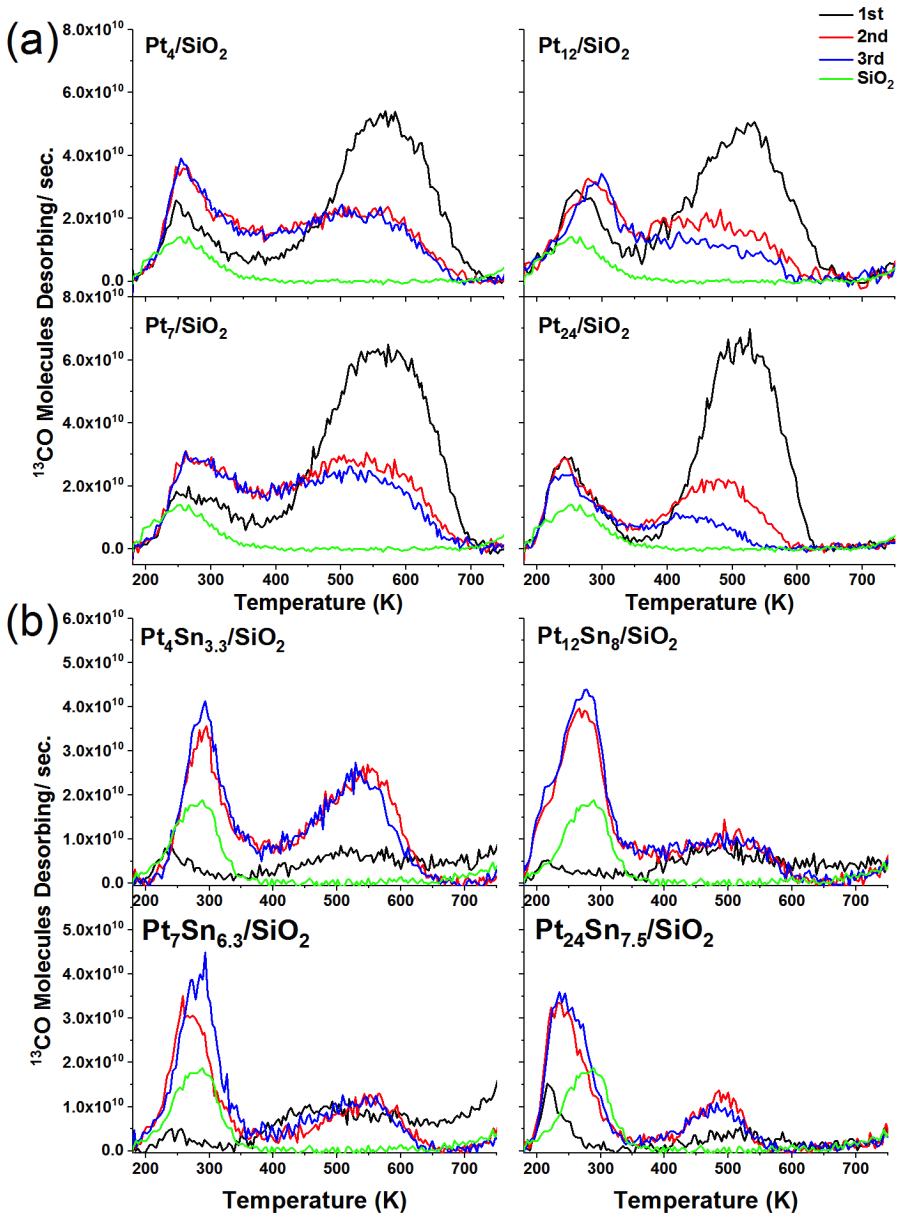

Figure 3. (a) Three consecutive ^{13}CO TPD spectra for as-deposited Pt_n/SiO_2 (n = 4, 7, 12, and 24). ^{13}CO from Pt-free SiO_2 is also shown (green). (b) Three sequential ^{13}CO TPD spectra for one $H_2/SnCl_4/H_2$ ALD cycle over $Pt_4Sn_{3.3}/SiO_2$, $Pt_7Sn_{6.3}/SiO_2$, $Pt_{12}Sn_8/SiO_2$, and $Pt2_4Sn_{7.5}/SiO_2$. For reference, the 2nd CO TPD from $H_2/SnCl_4/H_2$-SiO_2 is shown to reflect CO binding sites on the SiO_2 substrate (green).

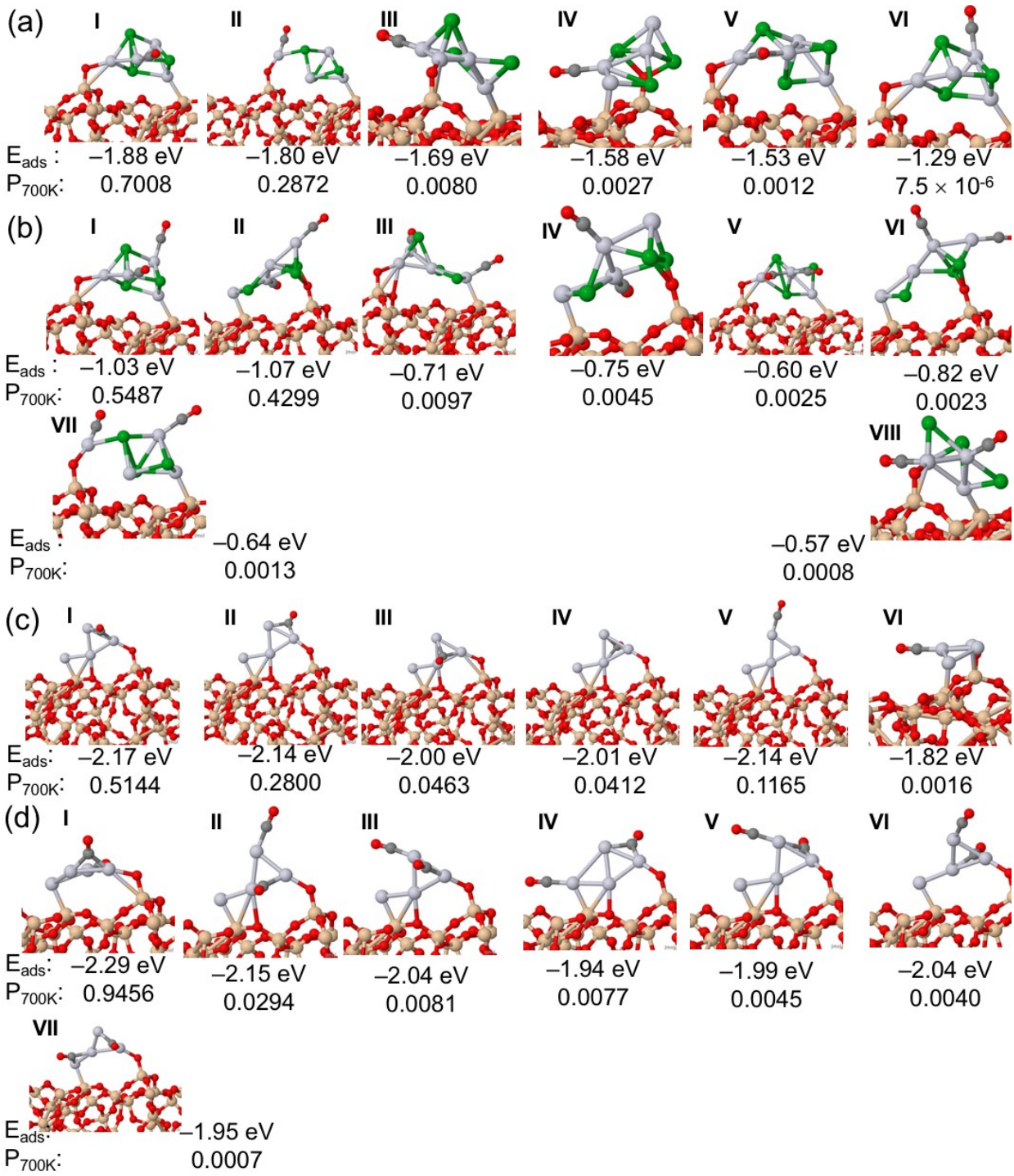

Figure 4. Local minima structures of (a) $CO/Pt_4/SiO_2$, (b) $(CO)_2/Pt_4/SiO_2$, (c) $CO/Pt_4Sn_3/SiO_2$, (d) $(CO)_2/Pt_4Sn_3/SiO_2$, obtained from global optimization. CO Adsorption energy (E_{ads}) and the Boltzmann population at 700 K (P_{700K}) are written below each structure. Note that for $(CO)_2/Pt_4/SiO_2$ and $(CO)_2/Pt_4Sn_3/SiO_2$, the adsorption energy corresponding to the second CO is shown (second adsorption energy).

Note that the rapid disappearance of Pt sites under CO binding in TPD suggests sintering that is faster than seen by TD-ISS and TD-XPS. For example, in ISS and XPS, Pt_4 sintered to a size between 12 and 24 (**Fig. 2**), but after the 2nd CO TPD it is able to bind less CO than as-prepared Pt_{24}, i.e. presumably became even larger. We calculated the dissociation energy of a Pt atom from Pt_4, and of PtCO from Pt_4CO, to assess if CO could facilitate sintering beyond thermal. Indeed, DFT calculations show that CO makes the Pt detachment from the cluster easier; whether the detached Pt atom ends up on SiO_2 surface or goes into the gas phase (**Note S3**). Hence, we infer that CO facilitates the monomer detachment from the pure Pt clusters, and speeds up Ostwald ripening. We additionally estimated the rates of Pt atoms evaporating to the gas phase to be negligible (**Note S3**).

Table 3. First and second CO binding energies on Pt_4/SiO_2 and Pt_4Sn_3/SiO_2 calculated at relevant temperatures. Note that all of the values obtained using the ensemble average representation formula based on the Boltzmann populations.

Cluster	$E_{bind,1}$(eV)		$E_{bind,2}$(eV)	
	450 K	700 K	450 K	700 K
Pt_4/SiO_2	–2.16	–2.15	–2.31	–2.30
Pt_4Sn_3/SiO_2	–1.89	–1.88	–1.06	–1.07

Evidently, Sn treatment significantly affects CO TPD. Most importantly, CO binding is slightly weaker than on pure Pt clusters (**Fig. 3**, **Table 3**), and from the 2nd to the 3rd CO TPD run more CO binding sites are preserved (**Fig. 3b**). For $Pt_4Sn_{3.3}/SiO_2$, the low temperature desorption features in the 2ndand

3rd TPD runs are similar to those observed in the 2nd run for Pt_4/SiO_2, and the high temperature features for $Pt_4Sn_{3.3}/SiO_2$ also have similar intensity but are sharper. For $Pt_7Sn_{6.3}/SiO_2$, the low temperature features are sharper than those seen for Pt_7/SiO_2, but the integrated intensities are similar (**Table S1**), while the high temperature features have significantly lower intensities. For $Pt_{12}Sn_8$ and $Pt_{24}Sn_{7.5}$, the results are similar to the smaller cluster sizes, in that run to run stability is maintained (unlike the bare Pt_{12}/SiO_2 and Pt_{24}/SiO_2). While the low temperature features are comparable to $Pt_4Sn_{3.3}$ and $Pt_7Sn_{6.3}$, the high temperature peaks are significantly attenuated.

The corresponding integrated CO desorption values are lower for Pt_nSn_x, compared to Pt_n. In the 2nd CO TPD, only 0.38 CO/Pt atom desorbed from $Pt_4Sn_{3.3}/SiO_2$ (compare to 0.49 CO/Pt for Pt_4), and 0.25 CO/Pt desorbed from $Pt_7Sn_{6.3}/SiO_2$ (compare to 0.56 for Pt_7/SiO_2). The Pt_4Sn_3 structures (**Fig. 1**) have Sn atoms on the surface that might partially block CO access to Pt. Additionally, Sn majorly effects the electronic structure of the clusters, making Pt atoms more negatively charged, and changing the ground state from triplet to singlet, and that also likely affects CO binding. For the larger clusters with a higher Pt:Sn stoichiometry, Pt_{12}/SiO_2 compared to $Pt_{12}Sn_8/SiO_2$ saw a drop from 0.41 to 0.30 CO/Pt, and Pt_{24}/SiO_2 compared to $Pt_{24}Sn_{7.5}/SiO_2$ saw a drop from 0.31 to 0.21 CO/Pt. Again, fewer CO binding sites were lost, when compared to the pure Pt clusters

The 2nd CO TPD data for $Pt_4Sn_{3.3}/SiO_2$ was fit to extract the distribution of desorption energies for CO (**Fig. S11**). The E_{des} distribution high energy

cut-off is just above 1.8 eV, compared to over 2.0 eV and 1.9 eV, respectively, for the 1st and 2nd TPD runs on Pt_4/SiO_2. The peak of the E_{des} distribution for $Pt_4Sn_{3.3}/SiO_2$ is ~1.65 eV, similar to the ~1.7 eV peak observed for Pt_4/SiO_2. This agrees with calculations (**Table 3**, **Note S4**). Because the clusters are saturated with CO in the experiment, with ~4.8 CO molecules desorbing *per* Pt_4 (including low temperature peripheral sites) in the 1st TPD run, and ~2 CO *per* $Pt_4Sn_{3.3}$ in the 2nd and subsequent TPD runs, the best comparison is between the DFT calculation for a single CO, and the high temperature limit of the experimental desorption. For Pt_4/SiO_2, the experimental limit is ~2.0 eV, which compares well with the 2.05 eV ensemble-averaged value for one CO on Pt_4/SiO_2. For $Pt_4Sn_{3.3}/SiO_2$, the experimental desorption limit is ~1.8 eV, again in excellent agreement with the ensemble-averaged value of ~1.88 eV. Note that the ensemble-average binding energy of the second CO on Pt_4/SiO_2 is actually ~0.15 eV larger than the binding energy for the first CO (**Fig. 4b**), whereas for Pt_4Sn_3/SiO_2, all CO binding is weakened, and the binding energy of the second CO is ~0.8 eV smaller than the first CO (**Table 3**). The decrease mainly results from the electronic differences of the binding sites in alloyed clusters (see Bader charges in **Fig. 1**), rather than repulsive lateral interactions between the two adsorbed CO molecules. Also, there is a geometric difference: CO preferentially binds to bridge sites on Pt_4/SiO_2, but on Pt_4Sn_3/SiO_2 it binds atop a single Pt atom, because as Pt and Sn mix, many Pt-Pt bonds and bridge sites are removed in PtSn alloys. These findings are in agreement with

Koel *et al.* who reported that that 0.33 ML Sn on Pt(111) reduces the binding energy of CO by a few kcal/mol, and the binding is only to Pt and not to Sn at temperatures of up to 300 K.[60] The main differences is that for Pt_4/SiO_2 in the 2nd TPD run, the distribution is substantially broadened to low energies, whereas the 2nd run for $Pt_4Sn_{3.3}/SiO_2$ has an E_{des} distribution that is relatively sharp, and as shown in **Fig. 6**, it does not broaden significantly in the 3rd TPD run.

Overall, we see that Sn suppresses sintering of Pt clusters, and its effect is more pronounced, as well as practically more important when the adsorbates are present. To additionally probe the proposed acceleration of sintering due to CO binding for pure clusters, and its deceleration for cluster alloys, we carried out TD-ISS experiments with adsorbed CO. **Fig. 5** shows TD-ISS data (points connected by lines) for Pt_4 and Pt_{12}. For comparison, the TPD data for the first and second TPD runs on Pt_4 and Pt_{12} samples are reproduced from **Fig. 3a**. Pt_4/SiO_2 and Pt_{12}/SiO_2 samples were prepared by cluster deposition, exposed to saturation doses of CO at 180 K, and then probed by ISS as the samples were heated to desorb the CO. The data from this first TD-ISS run are indicated by solid black circles. To probe ISS during a second CO TPD, while minimizing damage from the ISS beam, separate samples were prepared, subjected to a single CO TPD run (as in **Fig. 3**), then re-exposed to CO at 180 K and analyzed by TD-ISS (red solid triangles).

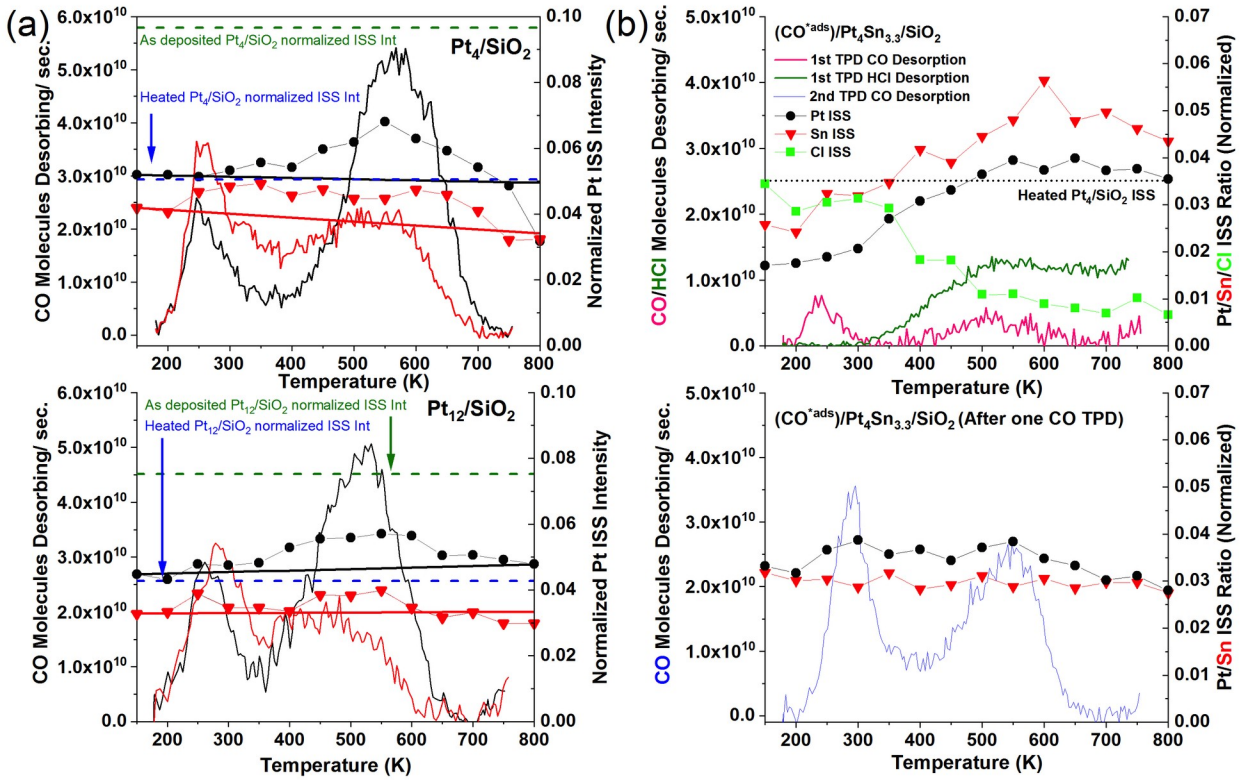

Figure 5. (a) (Black, solid circles) TD-ISS for as-deposited Pt_4/SiO_2 (top) and Pt_{12}/SiO_2 (bottom) with CO adsorbed. (Red, solid triangles) TD-ISS for Pt_4/SiO_2 and Pt_{12}/SiO_2 that have undergone one CO TPD followed by a second CO dose. For reference, the first (black) and second (red) CO TPDs are plotted. For comparison, the onset normalized Pt ISS intensities for as deposited (green dash) and heated (to 800 K – blue dash) Pt_4/SiO_2 are shown. (b) CO-TD ISS for as-prepared $Pt_4Sn_{3.3}/SiO_2$ (top) and $Pt_4Sn_{3.3}/SiO_2$ after it has undergone one CO TPD and was re-exposed to CO at 180 K (bottom). In both black circles and red triangles indicate Pt and Sn ISS intensities, respectively, and green squares show the Cl ISS intensity, which is only seen in the 1st run. For reference the TPD data for CO and HCl (1st run only) are shown.

First consider the TD-ISS taken in the 1st heat ramp after CO exposure on as-deposited Pt_n/SiO_2. Compared to the as-deposited Pt ISS intensities (green dashed lines), the intensities for the CO-saturated samples (blue dashed lines), were attenuated by ~50% for Pt_4 and by ~45% for Pt_{12}, due to

shadowing and blocking of He^+ scattering from Pt atoms by adsorbed CO. There was no significant change in Pt ISS as the samples were heated to ~350 K, while CO desorbs from the low energy sites seen in CO TPD, which are therefore not located on top of the clusters. Similar behavior has been seen for Pt_n/alumina[34] and Pd_n on both TiO_2[56] and alumina.[61] Then, as the temperature increased to 550 – 600 K, there was a significant increase in the ISS Pt signal, indicating that more strongly bound CO vacated Pt sites. At 600 K and above, however, the Pt signal declined substantially, despite additional CO desorption. This decrease is consistent with thermally-driven sintering. The sloping solid black lines show the Pt intensity from control experiments in which separate samples were cooled to 180 K, exposed to CO, and then held at 180 K during repeated ISS scans, i.e., these show the Pt signal change to do a combination of He^+ sputtering of both CO and Pt.

For TD-ISS carried out after a single CO TPD (red points, red lines showing control experiments with no heating), similar behavior is seen. There is a small amount of signal recovery, in this case starting as the low temperature CO component is desorbed, but then at high temperatures the signal drops again, reaching the value corresponding to the end of the control experiments. The smaller changes in Pt ISS signal in TD-ISS carried out after a CO TPD run, suggest that the changes in cluster structure/size are smaller after an initial CO TPD, i.e., that the largest changes in sample structure occurs as the samples are initially heated.

Fig. 5b (top) shows analogous TD-ISS of as-prepared, unheated $Pt_4Sn_{3.3}/SiO_2$ given a 180 K CO dose. In this 1st run, the sample would have had H, Cl, and CO adsorbed, and ISS intensities are shown for Pt, Sn, and Cl, and for reference, the HCl and CO desorption measured during the 1st CO TPD on an identically prepared sample are also plotted. The bottom frame shows an experiment in which an as-prepared $Pt_4Sn_{3.3}/SiO_2$ sample was dosed with CO at 180 K, subjected to one CO TPD to 800 K (also desorbing H and Cl), then was re-dosed with CO at 180 K prior to the onset of TD-ISS experiment. Pt and Sn ISS intensities are plotted; no Cl ISS was observed. The 2nd CO TPD is also plotted for reference.

The initial Pt ISS intensity was ~0.018, corresponding to >80% attenuation compared to the initial Pt intensity of ~0.1 for as-deposited Pt_4/SiO_2. This large attenuation is not surprising, given that the Pt_4 clusters present the strongest binding sites for the Sn, H, Cl, and CO adsorbates. Note that Sn ISS is observed with intensity higher than that for Pt at all temperatures. Because different elements can have considerably different He^+ ion survival probabilities,[58,59,62,63] the Pt/Sn ISS ratio cannot be simply related to the Pt/Sn stoichiometry in the surface layer. Nonetheless, it is clear that the $Pt_4Sn_{3.3}/SiO_2$ sample has a substantial fraction of Sn in its surface layer (as seen by DFT as well). Cl ISS is also observed, as expected.

As the sample was heated, weakly bound CO would have desorbed below 300 K, but there was only slight recovery of Pt ISS intensity, whereas some recovery would be expected due to adsorbate removal by

sputtering.[32,56] Therefore, we conclude that this component of the CO is not bound on Pt atoms, probably because the Pt clusters were already saturated by H, Cl, and Sn prior to the CO exposure. There was some growth in the Sn intensity below 300 K, which could indicate that some CO is bound to Sn, but CO may also be bound to the SiO_2 support or around the periphery of the clusters. Peripheral CO sites desorbing at low temperatures have been inferred from previous TPD/TD-ISS studies for Pt_n/alumina, Pd_n/alumina and Pd_n/TiO_2, for example.[34,56,64] The Cl ISS is constant below ~350 K.

Between 300 and 600 K, both CO and HCl desorb, and the Cl ISS decreased to a negligible value by ~500 K. Both the Pt and Sn ISS intensities increased, as expected for removal of adsorbates from the surface of the clusters. Above 600 K, the Pt and Sn intensities began to decrease slowly, despite apparent continued desorption of HCl, however, this high temperature HCl signal has been shown to result from desorption from sample holder surfaces. Note that the decline in Pt ISS intensity above 550 K is much smaller than for the Pt_n/SiO_2 samples, where extensive sintering occurred in the first TPD. Here, the very slow decline of Pt and Sn ISS signal is consistent with the rate of signal loss typically seen in repeated ISS scans due to sputtering of metal atoms from the surface.[32,64]

Note also that the final Pt ISS intensity for $Pt_4Sn_{3.3}/SiO_2$ is substantially higher that observed at the end of the TD-ISS experiment on Pt_4/SiO_2 (**Fig. 5**), implying that heated $Pt_4Sn_{3.3}/SiO_2$ has a higher fraction of its Pt atoms in the surface layer than heated Pt_4/SiO_2 (horizontal dashed line) despite the

fact that $Pt_4Sn_{3.3}/SiO_2$ also has high Sn ISS intensity indicating the presence of Sn atoms in the top layer of the clusters. The low Pt intensity for heated Pt_4 is attributed to extensive sintering to form clusters where many Pt atoms are not in the top layer. The TD-ISS results for $Pt_4Sn_{3.3}/SiO_2$, therefore, imply that that Sn alloying reduces the tendency toward ripening/sintering at high temperatures.

CONCLUSIONS

Supported sub-nanometer Pt clusters are promising catalysts that conserve the precious metal, yet possess extraordinary catalytic properties. Their thermal stability is a great challenge, however. We used a combination of theory and experiment to show that nano-alloying with Sn dramatically enhances the thermal stability of SiO_2-deposited Pt clusters against sintering. The alloyed clusters feature strong mixing between Sn and Pt, and these atoms form polar covalent bonds with each other, manifested in quenched electronic spins. Spin quenching is related to the special selectivity of thermal dehydrogenation of alkane to alkenes demonstrated earlier.[27] Due to this strong binding, the dissociation of the clusters to put Pt atoms on the surface is suppressed, and thus, Ostwald ripening is strongly inhibited. The larger charge of PtSn clusters also binds them more strongly to the support, and should create barriers to cluster diffusion. Thus the DFT results suggest that sintering should be inhibited by several factors. In the presence of CO

adsorbates, pure supported Pt clusters sinter even more rapidly than without adsorbates. This is facilitated by strong CO-Pt binding, which restructures the clusters, breaks Pt-Pt bonds, and eases the PtCO dissociation in Ostwald ripening. Adding Sn suppressed CO-assisted sintering just as efficiently, showing that Sn is a highly promising nano-alloying agent for cluster catalyst stabilization.

ASSOCIATED CONTENT

Supporting Information Available:

Contains detailed experimental and computational methodology; all thermally accessible isomers of Pt_4 and Pt_4Sn_3; PDOS of singlet and triplet Pt_4/SiO_2; DOS and PDOS of Pt_4Sn_3/SiO_2 and Pt_4/SiO_2 global minimum; all thermally-accessible isomers of Pt/SiO_2, Pt_3/SiO_2, Sn/SiO_2, Pt_4Sn_2/SiO_2, Pt_3Sn_3/SiO_2; $Pt_{12}(CO)_8$ structures obtained from ab initio MD; E_{des} profile for CO on Pt_4/SiO_2; Run-to-run CO TPD of Pt_4/SiO_2 extended to different maximum temperatures; E_{des} profile for CO on $Pt_4Sn_{3.3}/SiO_2$; extended amorphous silica simulated with classical MD; Quantified molecules desorbing from samples in TPD; CO binding energy of all thermally accessible isomers of $CO/Pt_4/SiO_2$, $(CO)_2/Pt_4/SiO_2$, $CO/Pt_4Sn_3/SiO_2$, $(CO)_2/Pt_4Sn_3/SiO_2$ using two different density functionals, PBE and RPBE.

AUTHOR INFORMATION

Corresponding Authors

*(Scott L. Anderson, Anastassia N. Alexandrova) E-mails: anderson@chem.utah.edu, ana@chem.uscla.edu

ORCIDs

Scott L. Anderson: 0000-0001-9985-8178

Anastassia Alexandrova: 0000-0002-3003-1911

Borna Zandkarimi: 0000-0002-7633-132X

Timothy J. Gorey: 0000-0002-7491-9648

Guangjing Li: 0000-0001-9990-631X

Julen Munarriz: 0000-0001-6089-6126

Notes

The authors declare no competing financial interest.

All the XYZ coordinates of $PtSn/SiO_2$ clusters in this study can be found here: https://github.com/bzkarimi/ptsn-sio2

ACKNOWLEDGEMENT

The work was supported by the Air Force Office of Scientific Research under a Basic Research Initiative grant (AFOSR FA9550-16-1-0141). CPU resources at the DOD (Department of Defense) High Performance Computing Modernization Program including the U.S. Air Force Research Laboratory DoD Supercomputing Resource Center (AFRL DSRC), the U.S. Army Engineer Research and Development Center (ERDC), and the Navy Supercomputing Resource Center (Navy DSRC), were used to conduct the computational part of this work.

REFERENCES

(1) Gao, W.; Hood, Z. D.; Chi, M. Interfaces in Heterogeneous Catalysts:

Advancing Mechanistic Understanding through Atomic-Scale Measurements. *Acc. Chem. Res.* **2017**, *50*, 787–795.

(2) Schlögl, R. Heterogeneous Catalysis. *Angew. Chemie - Int. Ed.* **2015**, *54*, 3465–3520.

(3) Hansen, T. W.; Delariva, A. T.; Challa, S. R.; Datye, A. K. Sintering of Catalytic Nanoparticles: Particle Migration or Ostwald Ripening? *Acc. Chem. Res.* **2013**, *46*, 1720–1730.

(4) Parkinson, G. S.; Novotny, Z.; Argentero, G.; Schmid, M.; Pavelec, J.; Kosak, R.; Blaha, P.; Diebold, U. Carbon Monoxide-Induced Adatom Sintering in a Pd–Fe_3O_4 Model Catalyst. *Nat. Mater.* **2013**, *12*, 724–728.

(5) Lei, Y.; Mehmood, F.; Lee, S.; Greeley, J.; Lee, B.; Seifert, S.; Winans, R. E.; Elam, J. W.; Meyer, R. J.; Redfern, P. C.; Teschner, D.; Schlögl, R.; Pellin, M. J.; Curtiss, L. A.; Vajda, S. Increased Silver Activity for Direct Propylene Epoxidation via Subnanometer Size Effects. *Science* **2010**, *328*, 224–228.

(6) Campbell, C. T. The Energetics of Supported Metal Nanoparticles: Relationships to Sintering Rates and Catalytic Activity. *Acc. Chem. Res.* **2013**, *46*, 1712–1719.

(7) Tabib Zadeh Adibi, P.; Pingel, T.; Olsson, E.; Grönbeck, H.; Langhammer, C. Pt Nanoparticle Sintering and Redispersion on a Heterogeneous Nanostructured Support. *J. Phys. Chem. C* **2016**, *120*, 14918–14925.

(8) Lee, S.; Seo, J.; Jung, W. Sintering-Resistant Pt@CeO_2 Nanoparticles for High-Temperature Oxidation Catalysis. *Nanoscale* **2016**, *8*, 10219–10228.

(9) Wichner, N. M.; Beckers, J.; Rothenberg, G.; Koller, H. Preventing Sintering of Au and Ag Nanoparticles in Silica-Based Hybrid Gels Using Phenyl Spacer Groups. *J. Mater. Chem.* **2010**, *20*, 3840–3847.

(10) Gorey, T. J.; Dai, Y.; Anderson, S. L.; Lee, S.; Lee, S.; Seifert, S.; Winans, R. E. Selective Growth of Al2O3 on Size-Selected Platinum Clusters by Atomic Layer Deposition. *Surf. Sci.* **2020**, *691*, 121485.

(11) Ha, M. A.; Dadras, J.; Alexandrova, A. Rutile-Deposited Pt-Pd Clusters: A Hypothesis Regarding the Stability at 50/50 Ratio. *ACS Catal.* **2014**, *4*, 3570–3580.

(12) Graham, G. W.; Jen, H.-W.; Ezekoye, O.; Kudla, R. J.; Chun, W.; Pan, X. Q.; McCabe, R. W. Effect of Alloy Composition on Dispersion Stability and Catalytic Activity for NO Oxidation over Alumina-Supported Pt–Pd Catalysts. *Catal. Letters* **2007**, *116*, 1–8.

(13) Dadras, J.; Jimenez-Izal, E.; Alexandrova, A. N. Alloying Pt Sub-Nano-Clusters with Boron: Sintering Preventative and Coke Antagonist? *ACS Catal.* **2015**, *5*, 5719–5727.

(14) Ha, M. A.; Baxter, E. T.; Cass, A. C.; Anderson, S. L.; Alexandrova, A. N. Boron Switch for Selectivity of Catalytic Dehydrogenation on Size-

Selected Pt Clusters on Al_2O_3. *J. Am. Chem. Soc.* **2017**, *139*, 11568–11575.

(15) Jimenez-Izal, E.; Zhai, H.; Liu, J. Y.; Alexandrova, A. N. Nanoalloying MgO-Deposited Pt Clusters with Si to Control the Selectivity of Alkane Dehydrogenation. *ACS Catal.* **2018**, *8*, 8346–8356.

(16) Jimenez-Izal, E.; Liu, J.-Y.; Alexandrova, A. N. Germanium as Key Dopant to Boost the Catalytic Performance of Small Platinum Clusters for Alkane Dehydrogenation. *J. Catal.* **2019**, *374*, 93–100.

(17) Li, Q.; Fu, J.; Zhu, W.; Chen, Z.; Shen, B.; Wu, L.; Xi, Z.; Wang, T.; Lu, G.; Zhu, J.; Sun, S. Tuning Sn-Catalysis for Electrochemical Reduction of CO_2 to CO via the Core/Shell Cu/SnO_2 Structure. *J. Am. Chem. Soc.* **2017**, *139*, 4290–4293.

(18) Shi, L.; Deng, G.-M.; Li, W.-C.; Miao, S.; Wang, Q.-N.; Zhang, W.-P.; Lu, A.-H. Al2O3 Nanosheets Rich in Pentacoordinate Al^{3+} Ions Stabilize Pt-Sn Clusters for Propane Dehydrogenation. *Angew. Chemie Int. Ed.* **2015**, *54*, 13994–13998.

(19) Jang, E. J.; Lee, J.; Jeong, H. Y.; Kwak, J. H. Controlling the Acid-Base Properties of Alumina for Stable PtSn-Based Propane Dehydrogenation Catalysts. *Appl. Catal. A Gen.* **2019**, *572*, 1–8.

(20) Pham, H. N.; Sattler, J. J. H. B.; Weckhuysen, B. M.; Datye, A. K. Role of Sn in the Regeneration of Pt/γ-Al2O3 Light Alkane Dehydrogenation

Catalysts. *ACS Catal.* **2016**, *6*, 2257–2264.

(21) Lee, M.-H.; Nagaraja, B. M.; Lee, K. Y.; Jung, K.-D. Dehydrogenation of Alkane to Light Olefin over PtSn/θ-Al_2O_3 Catalyst: Effects of Sn Loading. *Catal. Today* **2014**, *232*, 53–62.

(22) Zhang, J.; Deng, Y.; Cai, X.; Chen, Y.; Peng, M.; Jia, Z.; Jiang, Z.; Ren, P.; Yao, S.; Xie, J.; Xiao, D.; Wen, X.; Wang, N.; Liu, H.; Ma, D. Tin-Assisted Fully Exposed Platinum Clusters Stabilized on Defect-Rich Graphene for Dehydrogenation Reaction. *ACS Catal.* **2019**, *9*, 5998–6005.

(23) Siri, G. J.; Ramallo-López, J. M.; Casella, M. L.; Fierro, J. L. G.; Requejo, F. G.; Ferretti, O. A. XPS and EXAFS Study of Supported PtSn Catalysts Obtained by Surface Organometallic Chemistry on Metals: Application to the Isobutane Dehydrogenation. *Appl. Catal. A Gen.* **2005**, *278*, 239–249.

(24) Pastor-Pérez, L.; Sepúlveda-Escribano, A. Low Temperature Glycerol Steam Reforming on Bimetallic PtSn/C Catalysts: On the Effect of the Sn Content. *Fuel* **2017**, *194*, 222–228.

(25) Gorey, T. J.; Zandkarimi, B.; Li, G.; Baxter, E. T.; Alexandrova, A. N.; Anderson, S. L. Preparation of Size- And Composition-Controlled Pt_nSn_x/SiO_2 (n = 4, 7, 24) Bimetallic Model Catalysts with Atomic Layer Deposition. *J. Phys. Chem. C* **2019**, *123*, 16194–16209.

(26) Parker, S. C.; Campbell, C. T. Kinetic Model for Sintering of Supported

Metal Particles with Improved Size-Dependent Energetics and Applications to Au on TiO_2(110). *Phys. Rev. B* **2007**, *75*, 35430–35444.

(27) Gorey, T.; Zandkarimi, B.; Li, G.; Baxter, E.; Alexandrova, Anastassia; Anderson, S. Coking-Resistant Sub-Nano Dehydrogenation Catalysts: Pt_nSn_x/SiO_2 (n = 4, 7). *ACS Catal.* **2020**, *10*, 4543–4558.

(28) Guangjing, L.; Zandkarimi, B.; Cass, A. C.; Gorey, T. J.; Allen, B. J.; Alexandrova, A. N.; Anderson, S. L. Sn-Modification of Pt7/Alumina Model Catalysts : Suppression of Carbon Deposition and Enhanced Thermal Stability. *J. Chem. Phys.* **2020**, *152*, 024702–024713.

(29) Zhang, Z.; Zandkarimi, B.; Alexandrova, A. N. Ensembles of Metastable States Govern Heterogeneous Catalysis on Dynamic Interfaces. *Acc. Chem. Res.* **2020**, *53*, 447–458.

(30) Zandkarimi, B.; Alexandrova, A. N. Surface-supported Cluster Catalysis: Ensembles of Metastable States Run the Show. *Wiley Interdiscip. Rev. Comput. Mol. Sci.* **2019**, *9*, e1420.

(31) Dadras, J.; Shen, L.; Alexandrova, A. Pt-Zn Clusters on Stoichiometric MgO(100) and TiO_2(110): Dramatically Different Sintering Behavior. *J. Phys. Chem. C* **2015**, *119*, 6047–6055.

(32) Baxter, E. T.; Ha, M. A.; Cass, A. C.; Alexandrova, A. N.; Anderson, S. L. Ethylene Dehydrogenation on $Pt_{4,7,8}$ Clusters on Al_2O_3: Strong Cluster Size Dependence Linked to Preferred Catalyst Morphologies. *ACS Catal.*

2017, *7*, 3322–3335.

(33) Lee, S.; Fan, C.; Wu, T.; Anderson, S. L. Hydrazine Decomposition over Ir_n/Al_2O_3 Model Catalysts Prepared by Size-Selected Cluster Deposition. *J. Phys. Chem. B* **2005**, *109*, 381–388.

(34) Roberts, F. S.; Kane, M. D.; Baxter, E. T.; Anderson, S. L. Oxygen Activation and CO Oxidation over Size-Selected Pt_n/Alumina/Re(0001) Model Catalysts: Correlations with Valence Electronic Structure, Physical Structure, and Binding Sites. *Phys. Chem. Chem. Phys.* **2014**, *16*, 26443–26457.

(35) Kresse, G.; Joubert, D. From Ultrasoft Pseudopotentials to the Projector Augmented-Wave Method G. *Phys. Rev. B* **1999**, *59*, 1758–1775.

(36) Perdew, J. P.; Burke, K.; Ernzerhof, M. Generalized Gradient Approximation Made Simple. *Phys. Rev. Lett.* **1996**, *77*, 3865–3868.

(37) Kresse, G.; Furthmüller, J. Efficient Iterative Schemes for Ab Initio Total-Energy Calculations Using a Plane-Wave Basis Set. *Phys. Rev. B* **1996**, *54*, 11169–11186.

(38) Kresse, G.; Furthmiiller, J. Efficiency of Ab-Initio Total Energy Calculations for Metals and Semiconductors Using a Plane-Wave Basis Set. *Comput. Mater. Sci.* **1996**, *6*, 15–50.

(39) Kresse, G.; Hafner, J. Ab Initio Molecular Dynamics for Liquid Metals. *Phys. Rev. B* **1993**, *47*, 558–561.

(40) Kresse, G.; Furthmüller, J. Ab Initio Molecular-Dynamics Simulation of the Liquid-Metal-Amorphous-Semiconductor Transition in Germanium. *Phys. Rev. B* **1994**, *40*, 14251–14271.

(41) Ugliengo, P.; Sodupe, M.; Musso, F.; Bush, I. J.; Orlando, R.; Dovesi, R. Realistic Models of Hydroxylated Amorphous Silica Surfaces and MCM-41 Mesoporous Material Simulated by Large-Scale Periodic B3LYP Calculations. *Adv. Mater.* **2008**, *20*, 4579–4583.

(42) Becke, A. D. Density-functional Thermochemistry. III. The Role of Exact Exchange. *J. Chem. Phys.* **1993**, *98*, 5648–5652.

(43) Lee, C.; Yang, W.; Parr, R. G. Development of the Colle-Salvetti Correlation-Energy Formula into a Functional of the Electron Density. *Phys. Rev. B* **1988**, *37*, 785–789.

(44) Vosko, S. H.; Wilk, L.; Nusair, M. Accurate Spin-Dependent Electron Liquid Correlation Energies for Local Spin Density Calculations: A Critical Analysis. *Can. J. Phys.* **1980**, *58*, 1200–1211.

(45) Stephens, P. J.; Devlin, F. J.; Chabalowski, C. F.; Frisch, M. J. Ab Initio Calculation of Vibrational Absorption and Circular Dichroism Spectra Using Density Functional Force Fields. *J. Phys. Chem.* **1994**, *98*, 11623–11627.

(46) Zhai, H.; Alexandrova, A. N. Local Fluxionality of Surface-Deposited Cluster Catalysts: The Case of Pt7 on Al2O3. *J. Phys. Chem. Lett.* **2018**,

9, 1696–1702.

(47) Zhai, H.; Alexandrova, A. N. Ensemble-Average Representation of Pt Clusters in Conditions of Catalysis Accessed through GPU Accelerated Deep Neural Network Fitting Global Optimization. *J. Chem. Theory Comput.* **2016**, *12*, 6213–6226.

(48) Tang, W.; Sanville, E.; Henkelman, G. A Grid-Based Bader Analysis Algorithm without Lattice Bias. *J. Phys. Condens. Matter* **2009**, *21*, 084204–084210.

(49) Sanville, E.; Kenny, S. D.; Smith, R.; Henkelman, G. Improved Grid-Based Algorithm for Bader Charge Allocation. *J. Comput. Chem.* **2007**, *28*, 899–908.

(50) Henkelman, G.; Arnaldsson, A.; Jónsson, H. A Fast and Robust Algorithm for Bader Decomposition of Charge Density. *Comput. Mater. Sci.* **2006**, *36*, 354–360.

(51) Yu, M.; Trinkle, D. R. Accurate and Efficient Algorithm for Bader Charge Integration. *J. Chem. Phys.* **2011**, *134*, 064111–064118.

(52) Wales, D. J.; Doye, J. P. K. Global Optimization by Basin-Hopping and the Lowest Energy Structures of Lennard-Jones Clusters Containing up to 110 Atoms. *J. Phys. Chem. A* **1997**, *101*, 5111–5116.

(53) Roberts, F. S.; Anderson, S. L.; Reber, A. C.; Khanna, S. N. Initial and Final State Effects in the Ultraviolet and X-Ray Photoelectron

Spectroscopy (UPS and XPS) of Size-Selected Pd_n Clusters Supported on TiO_2(110). *J. Phys. Chem. C* **2015**, *119*, 6033–6046.

(54) Dai, Y.; Gorey, T. J.; Anderson, S. L.; Lee, S.; Lee, S.; Seifert, S.; Winans, R. E. Inherent Size Effects on XANES of Nanometer Metal Clusters: Size-Selected Platinum Clusters on Silica. *J. Phys. Chem. C* **2017**, *121*, 361–374.

(55) Wagner, C. D.; Naumkin, A. V.; Kraut-Vass, A.; Allison, J. W.; Powell, C. J.; Rumble Jr., J. R. NIST X-Ray Photoelectron Spectroscopy Database. *NIST Stand. Ref. Database 20, Version 3.2 (Web Version)* **2000**.

(56) Kaden, W. E.; Kunkel, W. A.; Roberts, F. S.; Kane, M.; Anderson, S. L. CO Adsorption and Desorption on Size-Selected Pd_n/TiO_2(110) Model Catalysts: Size Dependence of Binding Sites and Energies, and Support-Mediated Adsorption. *J. Chem. Phys.* **2012**, *136*, 204705–204716.

(57) Kaden, W. E.; Kunkel, W. A.; Anderson, S. L. Cluster Size Effects on Sintering, CO Adsorption, and Implantation in Ir/SiO_2. *J. Chem. Phys.* **2009**, *131*, 114701–114715.

(58) Aizawa, M.; Lee, S.; Anderson, S. L. Deposition Dynamics and Chemical Properties of Size-Selected Ir Clusters on TiO_2. *Surf. Sci.* **2003**, *542*, 253–275.

(59) Rabalais, J. W. *Principles and Applications of Ion Scattering Spectrometry : Surface Chemical and Structural Analysis*; Wiley: New

York, 2003.

(60) Hightower, A.; Perez, M. D.; Koel, B. E. An IRAS Study of CO Bonding on Sn/Pt(111) Surface Alloys at Maximal Pressures of 10 Torr. *Surf. Sci.* **2009**, *603*, 455–461.

(61) Kane, M. D.; Roberts, F. S.; Anderson, S. L. Effects of Alumina Thickness on CO Oxidation Activity over Pd_{20}/Alumina/Re(0001): Correlated Effects of Alumina Electronic Properties and Pd_{20} Geometry on Activity. *J. Phys. Chem. C* **2015**, *119*, 1359–1375.

(62) Jacobs, J. -P.; Reijne, S.; Elfrink, R. J. M.; Mikhailov, S. N.; Brongersma, H. H.; Wuttig, M. Quantification of the Composition of Alloy and Oxide Surfaces Using Low-energy Ion Scattering. *J. Vac. Sci. Technol. A* **1994**, *12*, 2308–2313.

(63) Brongersma, H. H.; Draxler, M.; de Ridder, M.; Bauer, P. Surface Composition Analysis by Low-Energy Ion Scattering. *Surf. Sci. Rep.* **2007**, *62*, 63–109.

(64) Kane, M. D.; Roberts, F. S.; Anderson, S. L. Mass-Selected Supported Cluster Catalysts: Size Effects on CO Oxidation Activity, Electronic Structure, and Thermal Stability of Pdn/Alumina (N≤30) Model Catalysts. *Int. J. Mass Spectrom.* **2014**, *370*, 1–15.

TOC Graphics:

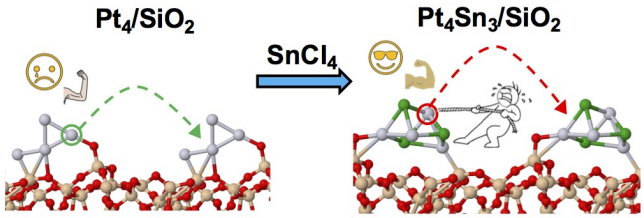
Pt_4/SiO_2
$SnCl_4$
Pt_4Sn_3/SiO_2